Microscopic observation of nonergodic states in two-dimensional nontopological bubble lattices

S. Pylypenko, M. Winter, U. K. Rößler, D. Pohl, R. Kyrychenko, Marein C. Rahn, B. Achinuq, J. R. Bollard, P. Vir, G. van der Laan, T. Hesjedal, J. Schultz, B. Rellinghaus, C. Felser, A. Lubk

Angaben zur Veröffentlichung / Publication details:

Pylypenko, S., M. Winter, U. K. Rößler, D. Pohl, R. Kyrychenko, Marein C. Rahn, B. Achinuq, et al. 2025. "Microscopic observation of nonergodic states in two-dimensional nontopological bubble lattices." Physical Review B 112 (21): 214424. https://doi.org/10.1103/ccxm-l6hx.

Editors' Suggestion | Featured in Physics

Microscopic observation of nonergodic states in two-dimensional nontopological bubble lattices

S. Pylypenko,[1,*,†] M. Winter,[2,3,*,‡] U. K. Rößler,[1] D. Pohl,[3] R. Kyrychenko,[1] M. C. Rahn,[4,5] B. Achinuq,[6] J. R. Bollard,[6,7] P. Vir,[2] G. van der Laan,[7] T. Hesjedal,[6,7] J. Schultz,[1] B. Rellinghaus,[3] C. Felser,[2,8] and A. Lubk[1,9,§]

[1]*Leibniz Institute for Solid State and Materials Research Dresden, Helmholtzstraße 20, 01069 Dresden, Germany*
[2]*Max Planck Institute for Chemical Physics of Solids, 01187 Dresden, Germany*
[3]*Dresden Center for Nanoanalysis, cfaed, TUD Dresden University of Technology, 01069 Dresden, Germany*
[4]*Institute for Solid State and Materials Physics, Technical University of Dresden, 01062 Dresden, Germany*
[5]*Experimental Physics VI, Center for Electronic Correlations and Magnetism, Institute of Physics, University of Augsburg, 86159 Augsburg, Germany*
[6]*Department of Physics, Clarendon Laboratory, University of Oxford, Oxford OX1 3PU, United Kingdom*
[7]*Diamond Light Source, Harwell Science and Innovation Campus, Didcot OX11 0DE, United Kingdom*
[8]*Würzburg-Dresden Cluster of Excellence ct.qmat, Technische Universität Dresden, 01062 Dresden, Germany*
[9]*Institute of Solid State and Materials Physics, TU Dresden, Haeckelstraße 3, 01069 Dresden, Germany*

(Received 24 March 2025; revised 14 October 2025; accepted 20 October 2025; published 11 December 2025)

Disordered two-dimensional (2D) lattices, including hexatic and various glassy states, are observed in a wide range of 2D systems including colloidal nanoparticle assemblies and fluxon lattices. Their disordered nature determines the stability and mobility of these systems, as well as their response to the external stimuli. Here we report on the controlled creation and characterization of a disordered 2D lattice of nontopological magnetic bubbles in the noncentrosymmetric ferrimagnetic alloy $Mn_{1.4}PtSn$. By analyzing the type and frequency of fundamental lattice defects, such as dislocations, the orientational correlation, as well as the induced motion of the lattice in an external field, a nonergodic glassy state, stabilized by directional application of an external field, is revealed.

DOI: 10.1103/ccxm-l6hx

I. INTRODUCTION

The collective behavior of elastic manifolds in a random or rough background, along with the formation of glassy states, remains a central topic within the broader study of glasses, amorphous materials, and other disordered configurations of condensed matter. An early motivation for this research was the behavior of dislocations under pinning by mixed sites in alloy crystals [1]. These systems, often trapped in nonergodic configurations, exhibit unique responses to external stresses, making their behavior particularly intriguing. The theories of dislocation-mediated melting in the context of the Berezinski-Kosterlitz-Thousless transition [2] provide a universal picture regarding the role of defect formation and plasticity due to quenched disorder, specifically for two-dimensional (2D) systems. Well studied examples in this context are vortex lattices in type-II superconductors [3,4], overlayers of colloidal particles [5,6], smectic [7] and blue phases of liquid crystals [8], or some phases of superfluidic helium [9–11].

2D magnetic bubble lattices, and skyrmion lattices in gyroptropic noncentrosymmetric ferromagnets, provide another example of such states, where the assembly of bubbles or skyrmions can be considered to form certain mesophases, intermediate between fully crystalline and liquid disordered states [12]. In 2D systems, the Mermin-Wagner theorem stipulates that fluctuations should preclude the formation of long-range ordered lattice states. However, in these magnetic systems, there are two effects promoting long-range order: first, the classical dipole-dipole interactions, owing to their long range, and, second, the magnetocrystalline anisotropy along with pinning in the regular crystalline lattice of the magnetic material. On the other hand, in a magnetic alloy, the atomistic disorder of the real structure creates a rough potential for the collective ordering of magnetic states via random anisotropies and random exchange forces [13], which can counteract these tendencies towards long-range order. Hence it is expected that magnetic bubble or skyrmion lattices in such a magnetic material behave quite differently compared to, e.g., a vortex lattice in a type-II superconductor, which allows one to study different effects.

Notably, quenched disorder and pinning determine the condensation of magnetic bubbles and skyrmions into a rich variety of (partly) ordered or disordered 2D lattices [12,14–16]. While interskyrmion or interbubble interaction typically prefers condensation into a periodic triangular lattice [17,18]

*These authors contributed equally to this work.
†Contact author: s.pylypenko@ifw-dresden.de
‡Contact author: Moritz.Winter@cpfs.mpg.de
§Contact author: a.lubk@ifw-dresden.de

(other regular lattices have been also observed [19]), quenching and random pinning can potentially lead to formation of glassy states (e.g., Bragg glass and vortex glass) [14,15,20], as observed in lattices of other building blocks [21], such as vortices in type-II superconductors [22] or colloidal particles [23]. It has been revealed that quenched disorder and pinning also determine the response (both static and dynamic) of magnetic skyrmions and bubbles under application of external stimuli [magnetic fields, electrical currents, and temperature (gradients)] [24,25]. While there is a considerable number of observations of disordered 2D lattices of magnetic skyrmions and bubbles in thin films (e.g., Refs. [14,26,27]), research mainly focused on interplay with magnetic frustration [28], geometric boundaries such as domain walls [29], and characterization of particular lattice defects such as grain boundaries [30], as well as characterization of the hexatic phase [31,32], while glassy states in skyrmion or bubble lattices remain less well studied.

Due to its rich phenomenology of magnetic structures and the intrinsic proliferation of crystallographic defects, the nonstoichiometric inverse half-Heusler compound $Mn_{1.4}PtSn$ offers a suitable platform to study disordered lattices. $Mn_{1.4}PtSn$ crystallizes in the space group $I\bar{4}2d$ and has been the focus of extensive research efforts for its multitude of magnetic textures, including lattices of magnetic solitons [33]. The noncentrosymmetric structure of $Mn_{1.4}PtSn$ gives rise to anisotropic Dzyaloshinskii-Moriya interaction (DMI) as well as a sizable uniaxial anisotropy. The competing magnetic interactions result in a large variety of magnetic textures, including nontopological bubbles, elliptical skyrmions, and antiskyrmions [33–35] that may be transformed into each other by applying (a sequence of) external magnetic fields of particular direction and strength. The large number of atomic vacancies and other lattice defects in $Mn_{1.4}PtSn$ provides a dense background of pinning sites, with their individual extension being small with respect to that of the magnetic textures in that material. Therefore, pinning is determined by the variation of the defect background rather than by individual pinning sites, which may be described by a slowly varying pinning potential.

In the following, we reveal a mechanism that exploits the rich landscape of metastable textures in combination with the random background potential to deliberately create a disordered lattice state of nontopological bubbles and skyrmions in $Mn_{1.4}PtSn$. Subsequently, we mainly characterize the bubble lattice state in terms of lattice defects, spatial correlations, and response to an external magnetic field.

II. CREATION OF DISORDERED NONTOPOLOGICAL BUBBLE LATTICE

Nonstoichiometric $Mn_{1.4}PtSn$ single crystals have been synthesized by a self-flux method as described in Ref. [36]. Subsequently, a thin, electron-transparent, lamella of approximately 100 nm thickness (lamella normal parallel to the c axis) has been prepared by focused ion beam (FIB) milling. The magnetic textures in the thin lamella were subsequently investigated with a JEOL F200 Transmission Electron Microscope that was operated in Lorentz mode [Lorentz Transmission Electron Microscopy (LTEM)]. In this mode, the objective lens is largely switched off to prevent field magnetization along the optical axis of the transmission electron microscope and the specimen plane is slightly defocused to observe magnetic phase contrast.

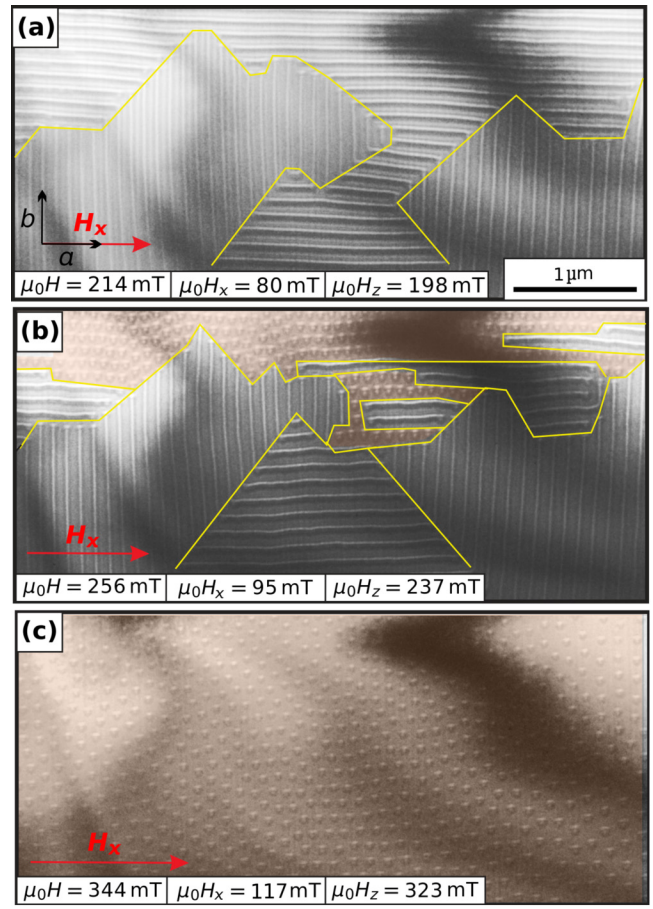

FIG. 1. Disordered bubble lattice state is stabilized by the application of increasing magnetic fields under an oblique angle of $\theta = 20°$. The field strengths are indicated as the full field strength $\mu_0 H$ and the respective components $\mu_0 H_x$ and $\mu_0 H_z$. (a) A mixed domain state of single-Q magnetic textures propagating along the a and b axis, respectively, is observed with a total applied field strength of $\mu_0 H = 214$ mT. The borders of the domains are indicated by yellow lines. (b) At $\mu_0 H = 256$ mT, the domain with its propagating vector aligned perpendicular to the in-plane field $\boldsymbol{H_x}$ partially transitions into a disordered bubble lattice. (c) Full sample coverage of the disordered bubble lattice is achieved at $\mu_0 H = 344$ mT.

2D lattices of magnetic bubbles have been created in the lamella by applying increasing magnetic fields (field direction fixed along the optical axis), while deliberately tilting the sample $\theta = 20°$ away from the c axis around the b axis. This allows adjustment of in- and out-of-plane magnetic fields with respect to the lamella. Upon increasing the external field, the initial helical state partially transforms into an intermediate homochiral state [Fig. 1(a)]. Subsequently, the initial helical state is partially transformed into a bubble state [Fig. 1(b)]. A complete magnetic bubble lattice appears above 344 mT as depicted in Fig. 1(c). In this transformation process, the disorder is introduced by the formation of irregular boundaries as well as spatially separated nucleation sites. The precise

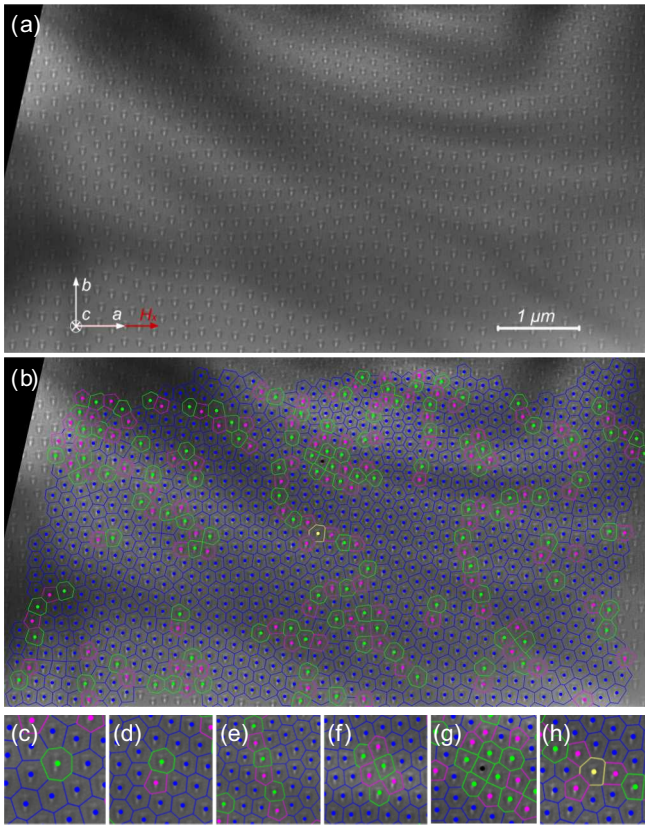

FIG. 2. (a) LTEM image of a 2D lattice of topologically trivial magnetic bubbles in $Mn_{1.4}PtSn$ observed at room temperature in an applied field of 344 mT under an angle of $\theta = 0.9^\circ$ with respect to the c axis. The crystal orientation and in-plane projection of the magnetic field due to the slight tilt of the sample around crystallographic a axes are indicated. (b) Nontopological bubble lattice in $Mn_{1.4}PtSn$. Solid dots denote the positions of the bubbles extracted from (a). The lattice sites are colored according to the number of nearest neighbors using the following scheme: four – black; five – pink; six – blue; seven – green; eight – yellow. The dominant deviation from the sixfold coordinated trigonal packing are fivefold and sevenfold coordinated defects. The bottom row shows zoom-outs of lattice defects within the generally hexagonal bubble lattice: (c) standalone seven neighbor bubble (disclination), (d) two bound disclinations with five (pink) and seven (green) neighbors forming a dislocation, (e) chain of dislocations forming a grain boundary, (f) twisted bond (two bound dislocations) bound to a dislocation, (g) an agglomeration of a four neighbor site and several seven neighbor sites, and (h) an agglomeration of an eight neighbor site and three five neighbor sites.

characterization of the intermediate states, as well as the boundaries between different magnetic textures, is the subject of a separate study.

Subsequently, to improve the LTEM contrast, the tilting angle was reduced to $\theta = 0.9^\circ$ while maintaining the applied field strength. The bubble lattice created by this protocol is relatively sparse, as evident in Fig. 2(a), with an average distance of $\approx$0.18 μm, significantly exceeding their individual sizes. As a result, their mutual interaction is primarily governed by long-range dipolar forces and rather weak, which generally promotes the formation of defects. Moreover, disorder does not impact the internal structure of the bubbles at lattice defects as, e.g., observed in densely packed lattices or defects [30].

III. CHARACTERIZATION OF THE DISORDERED BUBBLE LATTICE

In order to characterize the lattice, we determined the bubble positions in a first step by employing a pattern recognizing neural network. Partially annotated data from another experiment, featuring similar bubbles, was utilized for network training. Given the limited annotated data set, transfer learning was employed [37] utilizing the pretrained Efficient Det D2 768 × 768 model from the TensorFlow library. To detect new custom objects, we froze the section of the model responsible for identifying "features" in the image and fine-tuned the layers responsible for classifying those features into the desired objects. We furthermore note that the annotated training data set was sparse, i.e., not all existing objects in the images were annotated. Thus, to facilitate better learning, all regions potentially containing unannotated objects were filled with zero values. This was implemented to prevent the model from taking into account potentially misannotated areas. The image for bubble detection was significantly larger than the training images. Therefore, a sliding window approach was employed. This involved splitting the input image into smaller segments and the detection results from the model were aggregated into a unified outcome.

The result of this step is displayed in Fig. 2(b), where sixfold coordinated bubbles (standard case in triangular lattice) are colored blue, fivefold pink, and sevenfold green. Upon inspection of the coordination number, we observe that isolated five- or sevenfold coordinated bubbles, which correspond to disclinations [see Fig. 2(c)], are rarely present. Isolated bound five to seven defect pairs, i.e., dislocations [Fig. 2(d)], on the other hand, are occasionally observed within the lamella. Their proliferation (and the absence of disclinations) is characteristic for the hexatic phase [32]. When arranged as chains, dislocations form (large angle) grain boundaries [Fig. 2(e)]. The dislocation density along the one-dimensional trace of the boundary determines the character and angular mismatch of the adjacent well-ordered domains or grains. Straight and bent domain boundaries are the dominant type of defects observed throughout the lamella. Finally, we also observe twisted bonds composed of two adjacent edge dislocations (or more) with opposite Burgers vectors [Fig. 2(f)]. These lattice configurations correspond to local elastic deformations that typically occur in connection with grain boundaries. They may be formed in response to local stresses (e.g., due to local defects) or due to glide of dislocations on top of each other. Similarly, more complex and very rare lattice defects involving seven and four neighbor sites at highly distorted lattice regions may form at junctions of grain boundaries or highly frustrated lattice regions [Figs. 2(g) and 2(h)].

The nature of the observed defects, such as the domain boundaries, is further elucidated by mapping the phase of the complex local orientational order parameter of the observed lattice state (Fig. 3). For a 2D hexagonal lattice, the local orientational order parameter can be defined through the bond

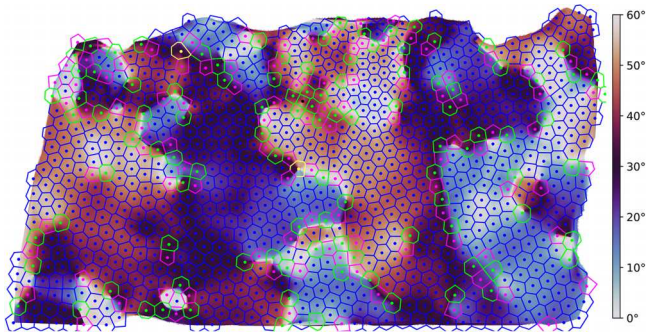

FIG. 3. Spatial orientation map of the bubble lattice. Lattice sites are color coded according to the number of nearest neighbors: four – black; five – pink; six – blue; seven – green; eight – yellow. The observed clusters (grains) are separated by chains of five to seven defects, identified previously.

orientations between nearest-neighboring sites [2]:

$$\Psi_6(\mathbf{r}_i) = \frac{1}{N_{nn}} \sum_{j}^{N_{nn}} e^{i6\Theta_{ij}}, \tag{1}$$

where N_{nn} represents the number of nearest-neighbor bubbles around the reference bubble located at position $\mathbf{r}_i$, which can be determined by Delaunay triangulation. Θ_{ij} is the angle between the ij bond and an arbitrary but fixed axis. The map of the phase of the order parameter $\arg[\Psi_6(\mathbf{r}_i)]/6$ exhibits the presence of grains separated by the previously observed grain boundaries as well as local orientation variations in the vicinity of localized defects. We note that sharp jumps from 60° to 0° stem from the $60° = 360°/6$ periodicity of the argument of the order parameter divided by 6.

Another perspective on the 2D lattice state is obtained by analyzing the structure factor of the whole field of view [Fig. 4(a)]. In the following the structure factor is computed from the bubble positions $\mathbf{R}_j$ by evaluating

$$S(\mathbf{k}) = \frac{1}{N} \left| \sum_{j=1}^{N} e^{-i\mathbf{k}\mathbf{R}_j} \right|^2, \tag{2}$$

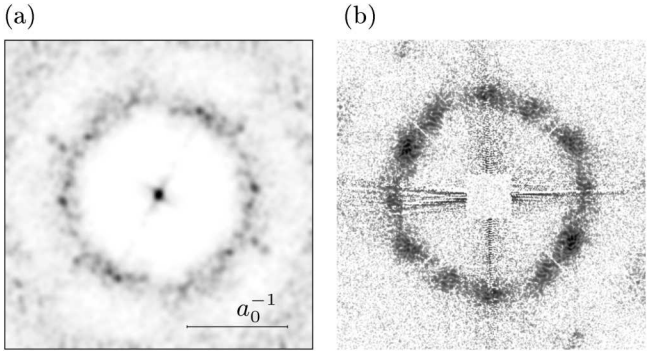

FIG. 4. (a) Structure factor of disordered bubble lattice computed from Eq. (2). (b) Transmission REXS diffraction pattern of a different lamella of similar geometry and in a slightly larger external magnetic field. Note that the sharp black lines along x and y, the sharp white lines along the diagonals, and the white square in the middle are due to the beam stop support.

where N denotes the total number of bubbles and $\mathbf{k}$ is the reciprocal lattice vector. In this definition the structure factor corresponds to the recorded intensity in a diffraction experiment on point-like scatterers [38].

The structure factor reveals a diffuse ring of first order without or very faint systematic reflections from larger sixfold symmetric grains, and a faintly visible ring of second order, indicating the absence of long range orientational order. To corroborate this finding, we also show a diffracted intensity from resonant elastic x-ray scattering experiments (REXS) on a similar lamellae exposed to a similar magnetic field protocol that exhibits a similar diffusive ring (as well as faint reflections from larger sixfold symmetric grains). This REXS experiment, which has been carried out on the I10 beamline at DIAMOND Light Source (UK), using the portable octupole magnet system (POMS) [39], acquired diffracted intensities over an 8 μm × 8 μm specimen area, hence improving on the lattice site statistics compared to LTEM. The photon energy was tuned to the Mn L_3 edge (642.2 eV). Due to the wavelength needed for resonant scattering as compared to the magnetic lattice spacing (momentum transfer in the first Brillouin zone), the experiment was carried out in transmission (for further details on the REXS experiment we refer to Ref. [40]). The magnetic transformation path as well as the external field of 480 mT applied under an oblique angle $\theta = 30°$ in the REXS experiment deviated somewhat from those in the LTEM experiments. While the larger field may slightly increase the bubble spacing (and hence the tendency to disorder), the oblique angle difference as well as the slightly different magnetic field protocol and lamella geometry may lead to a slightly different disorder state, e.g., with respect to defect density and grain sizes. We therefore abstain from a more detailed interpretation of azimuthal intensity modulations in the REXS data (also noting that they partially, e.g., around the diagonal direction, are due to scattering artifacts of the beam stop).

From these observations we may already conclude that the lattice under consideration is not a completely disordered liquid. On the other hand, the lattice is not well-ordered either (i.e., no Bragg glass). We may, however, also exclude the hexatic phase, which would exhibit a smaller orientational disorder (e.g., visible through distinguishable systematic reflections). Furthermore, the distribution of defects does not correspond to a multigrain state composed of well-defined (i.e., separated by grain boundaries) grains of different orientation. These findings point towards the presence of a glassy state.

In order to further elucidate the nature of the observed lattice state, we evaluated the orientational correlation function (see Fig. 5) over the whole field of view depicted in Fig. 2(a) in the following. The orientational correlation function $G_6(r)$ is defined as

$$G_6(r) = \frac{1}{N_r} \sum_{(i,j)}^{N_r} \Psi_6(\mathbf{r}_i)\Psi_6^*(\mathbf{r}_j), \tag{3}$$

where N_r is the number of bubbles at distance $r = |\mathbf{r}_i - \mathbf{r}_j|$. The rather large oscillations of G_6 visible in Fig. 5 are due to the restricted field of view limiting the statistics toward large distances in particular.

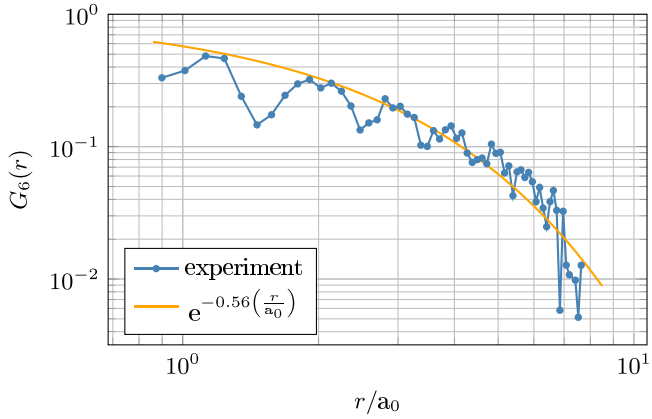

FIG. 5. Orientational correlation function $G_6(r)$ of the magnetic bubble lattice as a function of the normalized distance r/a_0 with a_0 being the mean bubble distance (blue curve). The orange curve represents an exponential fit to the data neglecting the local minima results in $G_6(r) = e^{-0.56(\frac{r}{a_0})}$.

The correlation function exhibits an exponential instead of an algebraic decay. This short range orientational correlation corroborates that the observed phase is not hexatic (exhibiting algebraic long-range orientational correlation). Moreover, the absence of long-range orientational correlation implies the absence of long-range translational correlation. Indeed, vortex glass phases, previously observed in superconducting vortex lattices [22], show a similar short range orientational order. The origin of the latter is the prevalence of dislocations, typically forming grain boundaries and twisted bonds. To gain further insight, we finally study how a change in the external magnetic field is deforming the observed lattice state.

IV. GLASS-LIKE MOTION

As discussed above, the nontopological bubble lattice in $Mn_{1.4}PtSn$ can be prepared by increasing the external magnetic field in a carefully chosen orientation. The resulting sequence of transformations of magnetic textures leads to a nonergodic state and rather large modulations of intermediate states. In the following, we study the impact of a small change of the external field. The small field change is facilitated by tilting the lamella by 0.8° around the y direction thereby increasing the field in the x direction by approximately 5 mT. The lattice positions before and after the increase of the in-plane field are depicted as blue and red dots in Fig. 6, respectively. Green and yellow dots mark lattice positions, where nontopological bubbles have been transformed into skyrmions—a transformation that has been reported previously for that sector of phase space in $Mn_{1.4}PtSn$ [34]. The difference between the lattice positions corresponds to their displacement resulting from this slight field change (Fig. 7).

The observed displacements average to 0.1 ± 10.7 nm in the x direction and 3.2 ± 15.8 nm in the y direction, respectively. The histogram depicted in Fig. 8 exhibits a roughly isotropic behavior. Accordingly, most of the displacements are well below one order of magnitude smaller than the average bubble distance. Larger displacements approaching one order of magnitude below the nearest neighbor distance occur at strongly confined regions of the lattice only.

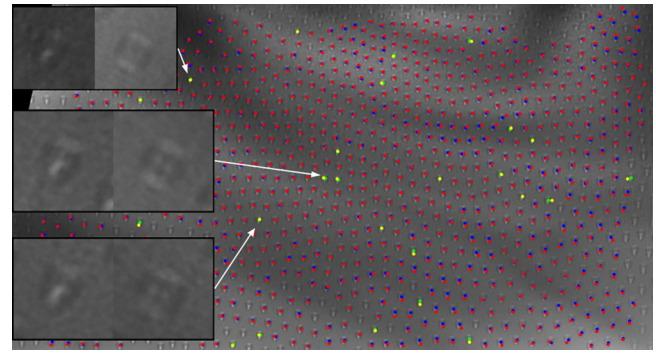

FIG. 6. Positions of bubbles and skyrmions at slightly different in-plane magnetic fields. Blue and red dots correspond to bubbles before and after application of additional in-plane field. Green and yellow dots indicate the positions of bubbles that transformed into skyrmions. Exemplary zoom-ins exhibit the transformation.

Such a strongly confined plastic motion is indicative of a glassy nonergodic state, where particles typically depin plastically, leading to large local distortions and shifts, while others remain pinned [12]. The depinning typically occurs in the vicinity of lattice defects such as grain boundaries. Indeed, we observe a weak correlation of plastic motion and defects in regions of small lattice defect density that are more stable than regions of large density. The strong pinning prohibits the ergodic exploration of all possible lattice configurations by thermal fluctuations.

Moreover, the absence of a significant correlation of the motion to the direction of the external field indicates that the local motion of the lattice is driven by a random force field generated by the distribution of crystalline defects (in analogy to film roughness as in the case of phenomenologically similar bubble lattices in ferrimagnetic Garnet films studied

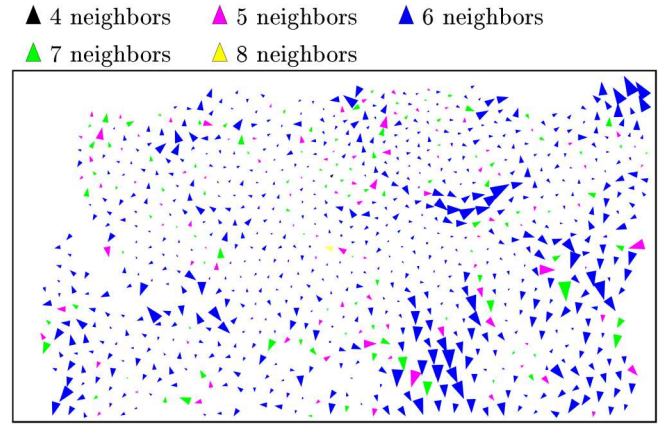

FIG. 7. Displacement of bubbles of the lattice shown in Fig. 2 upon slight variation of external magnetic field angle (by tilting the lamella). The size of the arrows is proportional to the displacement. Bubbles with six neighbors are depicted with blue arrows. Bubbles with five and seven neighbors are shown in purple and green, respectively. Black and yellow arrows correspond to four and eight neighbors, respectively.

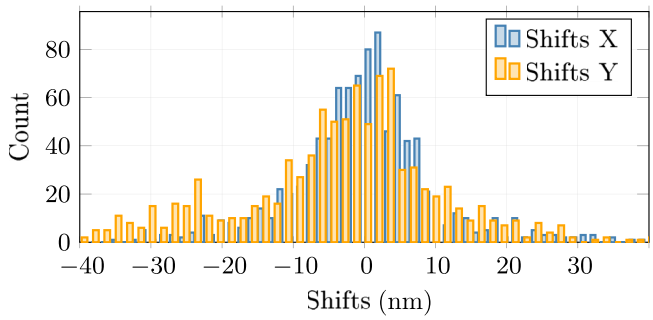

FIG. 8. Histogram of Cartesian displacement components of lattice positions along the x and y axes upon slight variation of external magnetic field angle. The average and width (standard deviations) of the distribution amount to 0.1 and 10.7 nm in x direction and 3.2 and 15.8 nm in y direction, respectively.

extensively in Refs. [14,15,24]). The role of crystal defects as pinning centers is further corroborated by the observation that the random shifts seem not to depend on the magnetic soliton being a bubble or skyrmion (Fig. 6). Note, however, that the small sample size does not allow a statistically significant corroboration of that observation.

V. SUMMARY

In summary, we have demonstrated a pathway for creating strongly disordered 2D lattices of nontopological magnetic bubbles in $Mn_{1.4}PtSn$. Herein, the disorder is imprinted by subsequent nucleation of different magnetic textures in an external magnetic field that are spatially separated by irregular boundaries. The shape and formation of these boundaries is likely influenced by the random background pinning potential originating from the large number of atomic lattice defects in this nonstoichiometric compound. The bubble lattice shows characteristics of a glass state in the locally observed lattice defects, the structure factor, and the exponential decay of the orientational correlation.

These results shed light on the general phenomenology of disordered magnetic skyrmion and bubble lattices, as pinning of the condensed nanoscale solitons by alloying disorder will, to some extent, always be present in real alloyed chiral helimagnetic systems. The induced plastic behavior of the lattice may be detrimental to applications aiming for the fast translation of bubble or skyrmion-based information units. On the other hand, stable storage of information may require that many different metastable configurations can be created and maintained over long times. Therefore, next steps towards such applications should concentrate on exploring dynamic response at various timescales and developing means to manipulate the observed glassy state in $Mn_{1.4}PtSn$.

ACKNOWLEDGMENTS

S.P. acknowledges support through the Philipp Schwartz Initiative of the Humboldt Foundation. M.W. acknowledges support from the International Max Planck Research School for Chemistry and Physics of Quantum Materials (IMPRS-CPQM). Work at TU Dresden and MPI CPfS was supported by the German Science Foundation (DFG) through CRC1143 (Project No. 247310070) and the Würzburg-Dresden Cluster of Excellence ct.qmat (EXC2147, Project No. 390858490). M.C.R. is grateful for support through the Emmy Noether programme of the DFG (Project No. 501391385). M.W., D.P., and B.R. are grateful for funding from the DFG through SPP2137 (Project No. 403503416). J.S. received funding from the HORIZON EUROPE framework program for research and innovation under Grant Agreement No. 101094299. The REXS measurements were conducted on the Portable Octupole Magnet System (POMS) on beamline I10 at the Diamond Light Source, UK, under Proposal No. MM28882. Financial support from the UK Skyrmion Project (Engineering and Physical Sciences Research Council, Grant No. EP/N032128/1) is gratefully acknowledged. J.R.B. acknowledges a Diamond-EPSRC studentship (Grants No. 2606404, No. EP/R513295/1, and No. EP/T517811/1).

A.L., B.R., and C.F. conceived the experiment. M.W. and D.P. performed the LTEM experiment. B.A., J.R.B., G.v.d.L., M.C.R., M.W., and T.H. performed the REXS experiment. S.P. and R.K. developed and applied machine-learning-based image processing tools to analyze the data. S.P., A.L., M.W., and U.K.R. analyzed and interpreted the data. P.V. synthesized the crystal. A.L., M.W., U.K.R., S.P., J.S., and M.C.R. prepared the manuscript with input from all authors.

DATA AVAILABILITY

The data that support the findings of this article are not publicly available upon publication because it is not technically feasible and/or the cost of preparing, depositing, and hosting the data would be prohibitive within the terms of this research project. The data are available from the authors upon reasonable request.

[1] R. Labusch, A statistical theory of solid solution hardening, Phys. Status Solidi B **41**, 659 (1970).

[2] J. V. José, L. P. Kadanoff, S. Kirkpatrick, and D. R. Nelson, Renormalization, vortices, and symmetry-breaking perturbations in the two-dimensional planar model, Phys. Rev. B **16**, 1217 (1977).

[3] D. S. Fisher, M. P. A. Fisher, and D. A. Huse, Thermal fluctuations, quenched disorder, phase transitions, and transport in type-II superconductors, Phys. Rev. B **43**, 130 (1991).

[4] G. Blatter, M. V. Feigel'man, V. B. Geshkenbein, A. I. Larkin, and V. M. Vinokur, Vortices in high-temperature superconductors, Rev. Mod. Phys. **66**, 1125 (1994).

[5] P. Tierno, Depinning and collective dynamics of magnetically driven colloidal monolayers, Phys. Rev. Lett. **109**, 198304 (2012).

[6] S. Deutschländer, T. Horn, H. Löwen, G. Maret, and P. Keim, Two-dimensional melting under quenched disorder, Phys. Rev. Lett. **111**, 098301 (2013).

[7] T. Bellini, L. Radzihovsky, J. Toner, and N. A. Clark, Universality and scaling in the disordering of a smectic liquid crystal, Science **294**, 1074 (2001).

[8] O. Henrich, K. Stratford, D. Marenduzzo, and M. E. Cates, Ordering dynamics of blue phases entails kinetic stabilization of amorphous networks, Proc. Natl. Acad. Sci. USA **107**, 13212 (2010).

[9] D. Osheroff, R. Richardson, and D. Lee, Evidence for a new phase of solid He 3, Phys. Rev. Lett. **28**, 885 (1972).

[10] G. Volovik, On Larkin-Imry-Ma state of 3He-A in aerogel, J. Low Temp. Phys. **150**, 453 (2008).

[11] J. Pollanen, J. Li, C. Collett, W. Gannon, W. Halperin, and J. Sauls, New chiral phases of superfluid 3He stabilized by anisotropic silica aerogel, Nat. Phys. **8**, 317 (2012).

[12] C. Reichhardt, C. J. O. Reichhardt, and M. V. Milošević, Statics and dynamics of skyrmions interacting with disorder and nanostructures, Rev. Mod. Phys. **94**, 035005 (2022).

[13] J. Kindervater, T. Adams, A. Bauer, F. X. Haslbeck, A. Chacon, S. Mühlbauer, F. Jonietz, A. Neubauer, U. Gasser, G. Nagy, N. Martin, W. Häußler, R. Georgii, M. Garst, and P. Pfleiderer, Evolution of magnetocrystalline anisotropies in $Mn_{1-x}Fe_xSi$ and $Mn_{1-x}Co_xSi$ as inferred from small-angle neutron scattering and bulk properties, Phys. Rev. B **101**, 104406 (2020).

[14] R. Seshadri and R. M. Westervelt, Statistical mechanics of magnetic bubble arrays, I. Topology and thermalization, Phys. Rev. B **46**, 5142 (1992).

[15] R. Seshadri and R. M. Westervelt, Statistical mechanics of magnetic bubble arrays. II. Observations of two-dimensional melting, Phys. Rev. B **46**, 5150 (1992).

[16] C. Reichhardt and C. J. O. Reichhardt, Depinning and nonequilibrium dynamic phases of particle assemblies driven over random and ordered substrates: a review, Rep. Prog. Phys. **80**, 026501 (2017).

[17] S. Mühlbauer, B. Binz, F. Jonietz, C. Pfleiderer, A. Rosch, A. Neubauer, R. Georgii, and P. Böni, Skyrmion lattice in a chiral magnet, Science **323**, 915 (2009).

[18] X. Z. Yu, Y. Onose, N. Kanazawa, J. H. Park, J. H. Han, Y. Matsui, N. Nagaosa, and Y. Tokura, Real-space observation of a two-dimensional skyrmion crystal, Nature (London) **465**, 901 (2010).

[19] R. Takagi, N. Matsuyama, V. Ukleev, L. Yu, J. S. White, S. Francoual, J. R. L. Mardegan, S. Hayami, H. Saito, K. Kaneko, K. Ohishi, Y. nuki, T.-h. Arima, Y. Tokura, T. Nakajima, and S. Seki, Square and rhombic lattices of magnetic skyrmions in a centrosymmetric binary compound, Nat. Commun. **13**, 1472 (2022).

[20] T. Giamarchi and P. Le Doussal, Elastic theory of flux lattices in the presence of weak disorder, Phys. Rev. B **52**, 1242 (1995).

[21] D. S. Fisher, Collective transport in random media: from superconductors to earthquakes, Phys. Rep. **301**, 113 (1998).

[22] J. Aragón Sánchez, R. Cortés Maldonado, N. R. Cejas Bolecek, G. Rumi, P. Pedrazzini, M. I. Dolz, G. Nieva, C. J. van der Beek, M. Konczykowski, C. D. Dewhurst, R. Cubitt, A. B. Kolton, A. Pautrat, and Y. Fasano, Unveiling the vortex glass phase in the surface and volume of a type-II superconductor, Commun. Phys. **2**, 143 (2019).

[23] A. Pertsinidis and X. S. Ling, Statics and dynamics of 2D colloidal crystals in a random pinning potential, Phys. Rev. Lett. **100**, 028303 (2008).

[24] R. Seshadri and R. M. Westervelt, Collective transport and shear flow of magnetic bubble arrays, Phys. Rev. B **47**, 8620 (1993).

[25] K. Litzius, J. Leliaert, P. Bassirian, D. Rodrigues, S. Kromin, I. Lemesh, J. Zazvorka, K.-J. Lee, J. Mulkers, N. Kerber, D. Heinze, N. Keil, R. M. Reeve, M. Weigand, B. V. Waeyenberge, G. Schütz, K. E.-Sitte, G. S. D. Beach, and M. Kläu, The role of temperature and drive current in skyrmion dynamics, Nat. Electron. **3**, 30 (2020).

[26] P.-J. Hsu, L. Rózsa, A. Finco, L. Schmidt, K. Palotás, E. Vedmedenko, L. Udvardi, L. Szunyogh, A. Kubetzka, K. von Bergmann, and R. Wiesendanger, Inducing skyrmions in ultrathin Fe films by hydrogen exposure, Nat. Commun. **9**, 1571 (2018).

[27] L. Wang, C. Liu, N. Mehmood, G. Han, Y. Wang, X. Xu, C. Feng, Z. Hou, Y. Peng, X. Gao, and G. Yu, Construction of a Room-Temperature Pt/Co/Ta multilayer film with ultrahigh-density skyrmions for memory application, ACS Appl. Mater. Interfaces **11**, 12098 (2019).

[28] K. Karube, J. S. White, D. Morikawa, C. D. Dewhurst, R. Cubitt, A. Kikkawa, X. Yu, Y. Tokunaga, T. Arima, H. M. Rønnow, Y. Tokura, and Y. Taguchi, Disordered skyrmion phase stabilized by magnetic frustration in a chiral magnet, Sci. Adv. **4**, eaar7043 (2018).

[29] H. Nakajima, A. Kotani, M. Mochizuki, K. Harada, and S. Mori, Formation process of skyrmion lattice domain boundaries: The role of grain boundaries, Appl. Phys. Lett. **111**, 192401 (2017).

[30] T. Matsumoto, Y.-G. So, Y. Kohno, H. Sawada, Y. Ikuhara, and N. Shibata, Direct observation of Σ7 domain boundary core structure in magnetic skyrmion lattice, Sci. Adv. **2**, e1501280 (2016).

[31] J. Rajeswari, P. Huang, G. F. Mancini, Y. Murooka, T. Latychevskaia, D. McGrouther, M. Cantoni, E. Baldini, J. S. White, A. Magrez, T. Giamarchi, H. M. Rønnow, and F. Carbone, Filming the formation and fluctuation of skyrmion domains by cryo-Lorentz transmission electron microscopy, Proc. Natl. Acad. Sci. USA **112**, 14212 (2015).

[32] P. Huang, T. Schönenberger, M. Cantoni, L. Heinen, A. Magrez, A. Rosch, F. Carbone, and H. M. Rønnow, Melting of a skyrmion lattice to a skyrmion liquid via a hexatic phase, Nat. Nanotechnol. **15**, 761 (2020).

[33] A. K. Nayak, V. Kumar, T. Ma, P. Werner, E. Pippel, R. Sahoo, F. Damay, U. K. Rößler, C. Felser, and S. S. P. Parkin, Magnetic antiskyrmions above room temperature in tetragonal Heusler materials, Nature (London) **548**, 561 (2017).

[34] L. Peng, R. Takagi, W. Koshibae, K. Shibata, K. Nakajima, T.-H. Arima, N. Nagaosa, S. Seki, X. Yu, and Y. Tokura, Controlled transformation of skyrmions and antiskyrmions in a non-centrosymmetric magnet, Nat. Nanotechnol. **15**, 181 (2020).

[35] J. Jena, B. Göbel, T. Ma, V. Kumar, R. Saha, I. Mertig, C. Felser, and S. S. P. Parkin, Elliptical bloch skyrmion chiral twins in an antiskyrmion system, Nat. Commun. **11**, 1115 (2020).

[36] P. Vir, N. Kumar, H. Borrmann, B. Jamijansuren, G. Kreiner, C. Shekhar, and C. Felser, Tetragonal superstructure of the antiskyrmion hosting heusler compound $Mn_{1.4}PtSn$, Chem. Mater. **31**, 5876 (2019).

[37] Q. Yang, Y. Zhang, W. Dai, and S. Pan, *Transfer Learning* (Cambridge University Press, Cambridge, UK, 2020).

[38] B. Warren, *X-ray Diffraction*, Addison-Wesley Series in Metallurgy and Materials Engineering (Dover Publications, Mineola, NY, 1990).

[39] G. van der Laan and A. I. Figueroa, X-ray magnetic circular dichroism—A versatile tool to study magnetism, Coord. Chem. Rev. **277–278**, 95 (2014).

[40] M. Winter *et al.*, Field-induced condensation of π to 2π soliton lattices in chiral magnets, arXiv:2508.10640.